Measuring the iron content of dopaminergic neurons in substantia nigra with MRI relaxometry: Supplementary Information

Malte Brammerloh[abc], Markus Morawski[d], Isabel Weigelt[d], Tilo Reinert[ac], Charlotte Lange[ac], Primož Pelicon[e], Primož Vavpetič[e], Steffen Jankuhn[c], Carsten Jäger[a], Anneke Alkemade[f], Rawien Balesar[f], Kerrin Pine[a], Filippos Gavriilidis[a], Robert Trampel[a], Enrico Reimer[a], Thomas Arendt[d], Nikolaus Weiskopf[act†], and Evgeniya Kirilina[aj†]

***For correspondence:**
mbrammerloh@cbs.mpg.de (MB)

[†]These authors contributed equally to this work

[a]Department of Neurophysics, Max Planck Institute for Human Cognitive and Brain Sciences, Stephanstr. 1a, 04103 Leipzig, Germany; [b]International Max Planck Research School on Neuroscience of Communication: Function, Structure, and Plasticity; [c]Felix Bloch Institute for Solid State Physics, Faculty of Physics and Earth Sciences, Leipzig University, Linnéstr. 5, 04103 Leipzig, Germany; [d]Paul Flechsig Institute of Brain Research, University of Leipzig, Liebigstr. 19, 04103, Leipzig, Germany; [e]Jožef Stefan Institute, Jamova 39, SI-1000 Ljubljana, Slovenia; [f]Integrative Model-based Cognitive Neuroscience Research Unit, University of Amsterdam, Amsterdam, Nieuwe Achtergracht 129B, 1001 NK Amsterdam, The Netherlands; [j]Center for Cognitive Neuroscience Berlin, Free University Berlin, Habelschwerdter Allee 45, 14195, Berlin, Germany

Supplementary Information

Estimation of the Susceptibility of Neuromelanin-Bound Iron

A monoatomic iron binding site with spin of $5/2$ was observed within neuromelanin in *substantia nigra* using electron paramagnetic resonance spectroscopy (***Zecca et al., 2004***). We therefore estimated neuromelanin's susceptibility per iron load by using Curie's law for monoatomic iron with spin $S = 5/2$.

$$\chi_{\mathrm{NM}} = \frac{\mu_0 S(S+1) g^2 \mu_{\mathrm{B}}^2}{3 k_{\mathrm{B}} T} = 3.275\,\mathrm{ppb/ppm},$$

where μ_0 is the vacuum permeability, $g = 2$ the Landé factor of the electron, μ_{B} the Bohr's magneton, k_{B} Boltzmann's constant and $T = 300\,\mathrm{K}$ the temperature. Note, that this value provides only a coarse approximation of the magnetic susceptibility of neuromelanin-bound iron since the structure of NM is known to be complex. Crystalline domains with unknown susceptibility were reported to be present within NM granules (***Sulzer et al., 2018***).

References

Sulzer D, Cassidy C, Horga G, Kang UJ, Fahn S, Casella L, Pezzoli G, Langley J, Hu XP, Zucca FA, Isaias IU, Zecca L. Neuromelanin detection by magnetic resonance imaging (MRI) and its promise as a biomarker for Parkinson's disease. NPJ Parkinson's Disease. 2018 Apr; 4(11). https://www.ncbi.nlm.nih.gov/pmc/articles/PMC5893576/, doi: 10.1038/s41531-018-0047-3.

Zecca L, Stroppolo A, Gatti A, Tampellini D, Toscani M, Gallorini M, Giaveri G, Arosio P, Santambrogio P, Fariello RG, Karatekin E, Kleinman MH, Turro N, Hornykiewicz O, Zucca FA. The role of iron and copper molecules in the neuronal vulnerability of locus coeruleus and substantia nigra during aging. Proceedings of the National Academy of Sciences of the United States of America. 2004 Jun; 101(26):9843–9848. doi: 10.1073/pnas.0403495101.

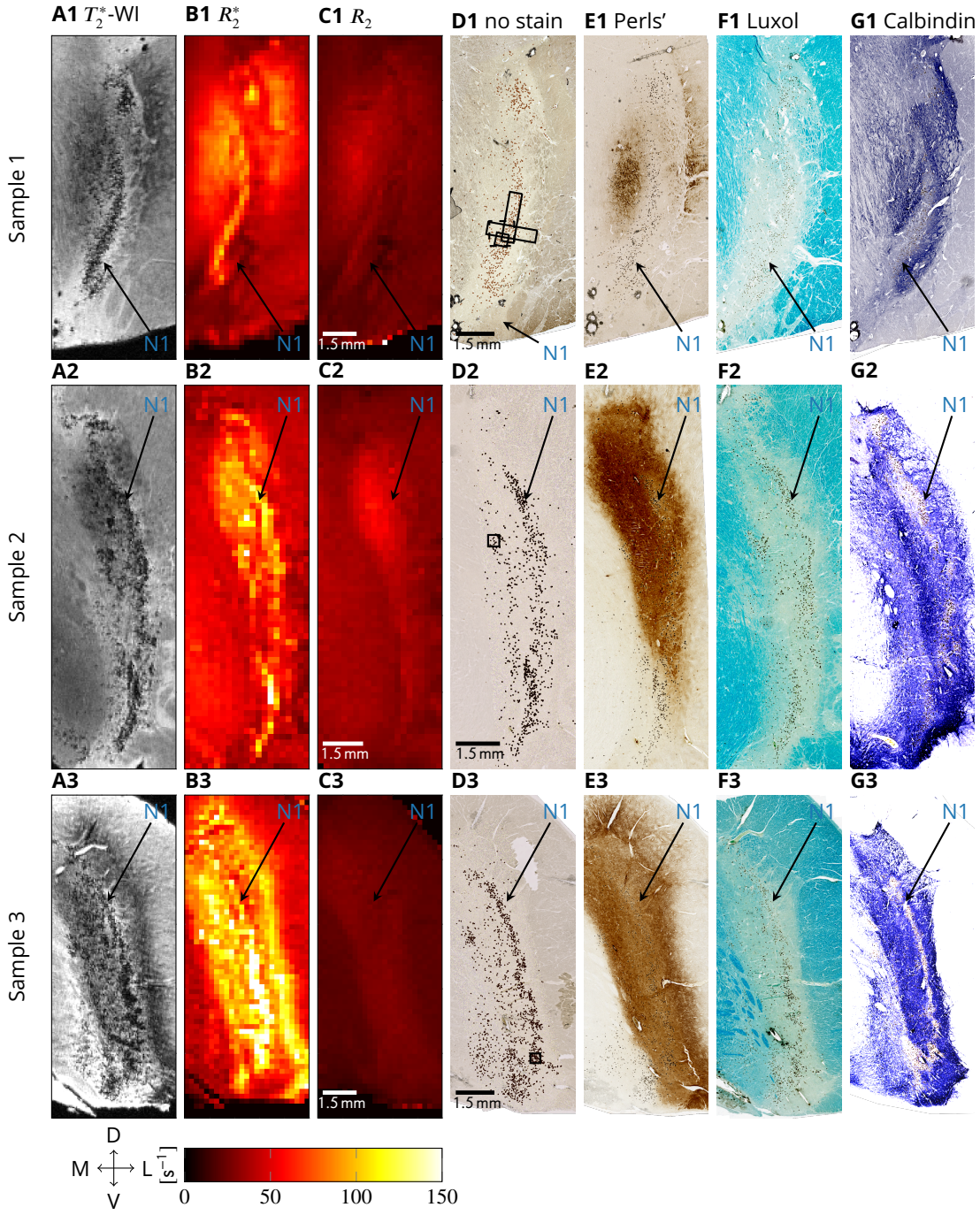

Figure S1. MRI and histology data on the three analyzed samples are presented in three rows. A1, A2, A3: T_2^*-WI show granular hypointensities in the nigrosomes, especially in N1. B1, B2, B3: On quantitative R_2^* maps, areas with high relaxation rates resemble the hypointensities in T_2^*-WI. C1, C2, C3: On quantitative R_2 maps, no nigrosome structure is visible. D1, D2, D3: Clusters of high neuromelanin density on unstained sections were co-localized with granular hypointensities in T_2^*-WI and hyperintensities on quantitative R_2^* maps. (Each neuromelanin domain was marked with a brown dot.) The PIXE measurement areas (Figs. 1, 3, S2) are indicated with a black squares. In sample 1, the dashed and solid squares indicate measurements on two adjacent histological sections. E1, E2, E3: On sections stained with Perls' solution for iron, a high intersubject variability was observed. F1, F2, F3: On sections stained with Luxol for myelin, a low staining intensity was observed in the DN-rich nigrosome areas. G1, G2, G3: On sections stained for calbindin, an elongated structure of low staining intensity was identified as N1. In all images, the location of N1 is indicated with an arrow. Anatomical directions are indicated as medial (M), lateral (L), ventral (V), and dorsal (D).

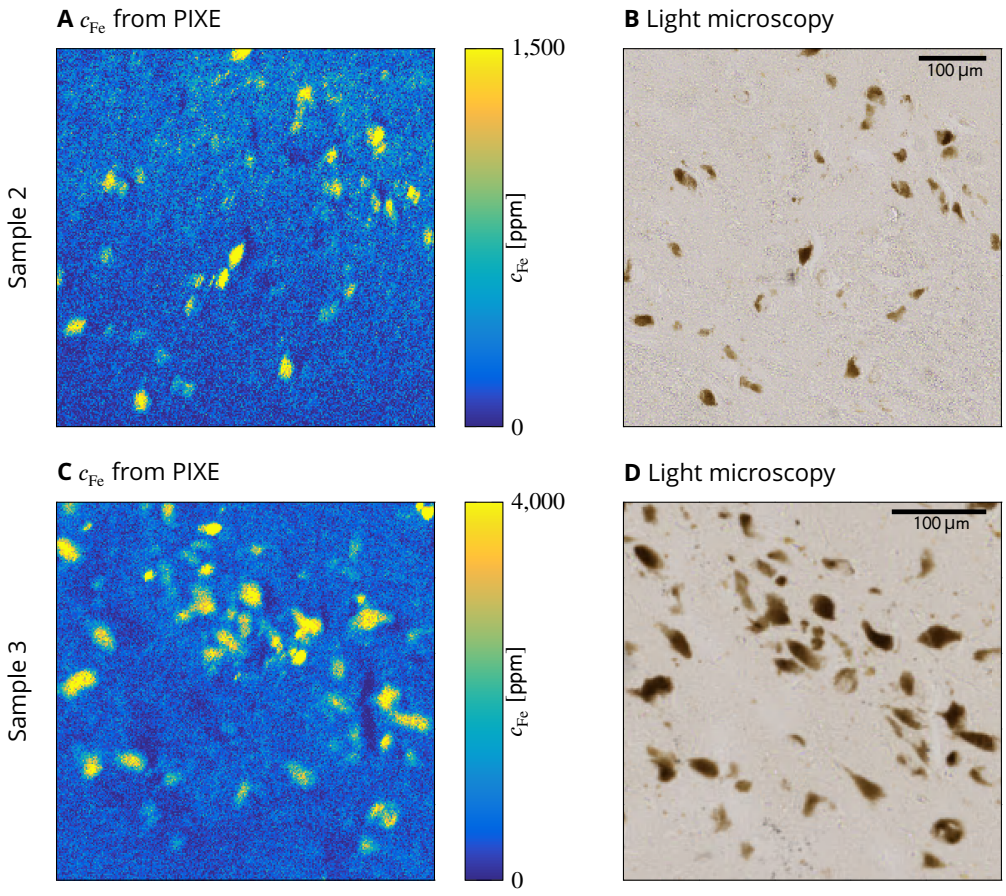

Figure S2. Iron concentration maps obtained with PIXE (A, C) together with light microscopy of the measurement area (B, D) in samples 2 (top row) and 3 (bottom). In all samples, neuromelanin domains in DN showed increased iron concentrations, while most iron was found outside of DN, probably associated with ferritin. In Table II we report the average iron concentration in neuromelanin-rich areas of DN as well as in the rest of the measurement area, the volume fraction of neuromelanin-rich areas, and the iron fraction in DN. The depicted areas are indicated in Fig. S1D2, D3.

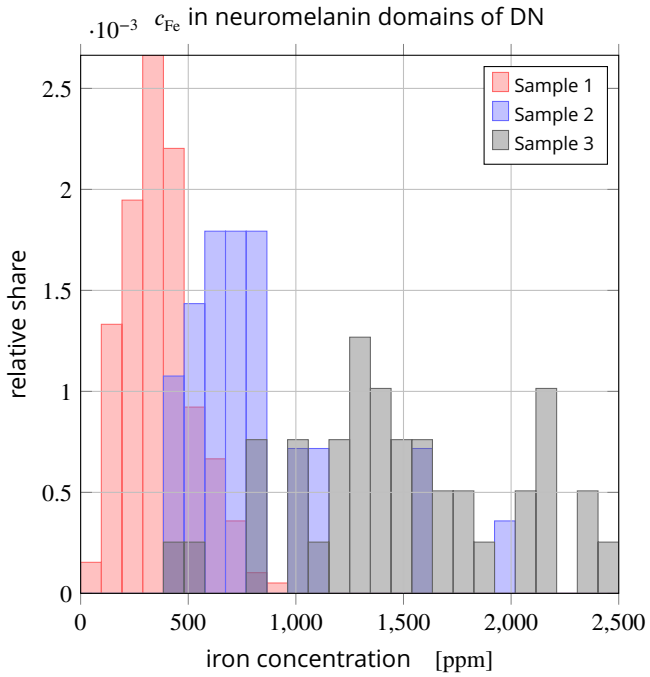

Figure S3. Histograms of iron concentrations in the neuromelanin of DN for all three samples. A high intersubject variability of $c_{Fe,NM}$ in DN is apparent: For sample 1, a mean and standard deviation of (365 ± 161) ppm was found, for sample 2 (811 ± 366) ppm, for sample 3 (1495 ± 499) ppm, where the mean and standard deviation are calculated across neurons.

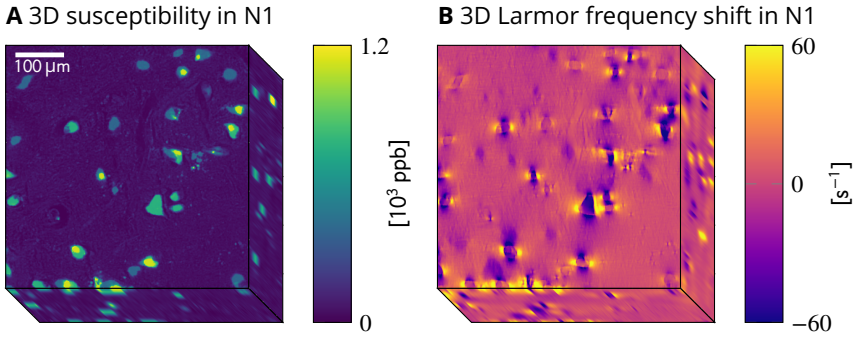

Figure S4. 3D susceptibility (A) and Larmor frequency shift maps (B) generated from the 3D quantitative iron map (Fig. 3D). DN show increased susceptibility and induce strong Larmor frequency perturbations in their vicinity.

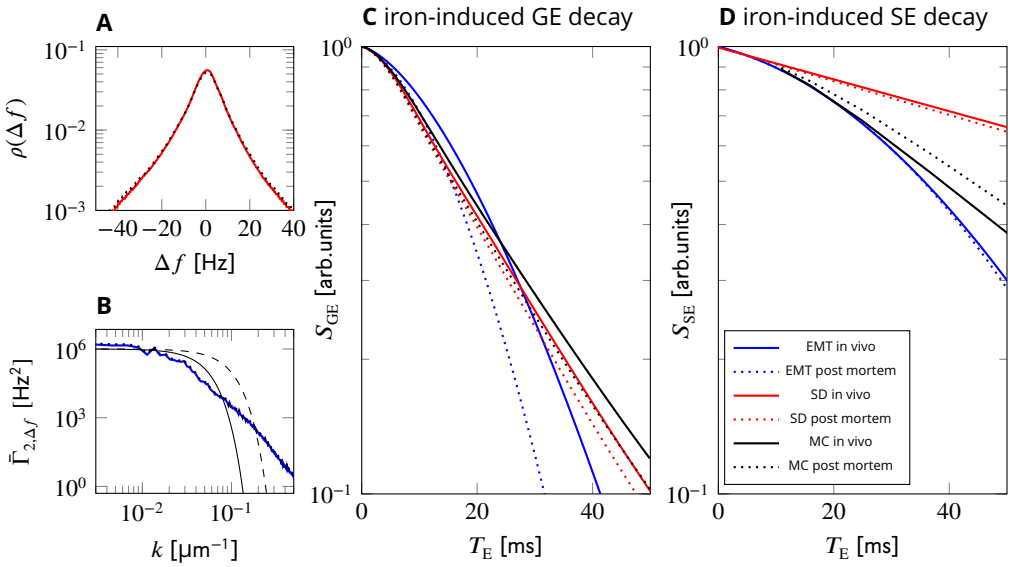

Figure S5. Modeling microscale relaxation in N1 of sample 1 in *in vivo* conditions. A: The increased temperature *in vivo* (310 K) reduces the width of the Larmor frequency shift histogram (red) slightly when compared to the *post mortem* histogram (black, dotted) (by $1 - 293\,\mathrm{K}/310\,\mathrm{K} \approx 5\,\%$). The susceptibility causes this because it is inversely proportional to the temperature according to Curie's law. B: The abscissa of the two-point corrleator (blue) is by a small factor $(1 - (293\,\mathrm{K}/310\,\mathrm{K})^2 \approx 11\,\%)$ lower than the *post mortem* two-point correlator (black, dotted). The increased diffusion coefficient *in vivo* accelerates the averaging over the higher spatial frequencies k, as the decreased width of the diffusion kernel at $T_E = 20\,\mathrm{ms}$ *in vivo* (black, solid) compared to *post mortem* (black, dashed) indicates. C: Despite the higher temperature and faster diffusion *in vivo* (solid lines), the GE decays predicted with Monte Carlo (MC, black) and in static dephasing (SD, red) are similar to the ones predicted for *post mortem* conditions (dotted). Hence, the relaxation regime is also *in vivo* close to static dephasing. Effective medium theory (EMT; blue, solid) differs substantially from EMT's prediction *post mortem* (blue, dotted) and MC. D: The SE decay predicted by MC in the *in vivo* condition is faster (black, solid) than *post mortem* (black, dotted). EMT predicts similar decays *in vivo* (blue, solid) and *post mortem* (blue, dotted), but overestimates the transverse relaxation rate.